Impact of grain microstructure on the heterogeneity of precipitation strengthening in an Al–Li–Cu alloy

Thomas Dorin, Alexis Deschamps, Frédéric de Geuser, Florence Robaut

Impact of grain microstructure on the heterogeneity of precipitation strengthening in an Al–Li–Cu alloy

Thomas Dorin [a,b,c,d,*], Alexis Deschamps [a,b], Frédéric De Geuser [a,b], Florence Robaut [e]

[a] Université Grenoble Alpes, SIMAP, F-38000 Grenoble, France
[b] CNRS, SIMAP, F-38000 Grenoble, France
[c] Institute for Frontier Materials, Deakin University, Geelong, Victoria 3217, Australia
[d] Constellium Technology Center, CS 10027, 38341 Voreppe Cedex, France
[e] Consortium des Moyens Technologiques Communs, Grenoble-INP, F-38502 St. Martin d'Hères, France

The effect of grain microstructure on the age-hardening behavior is investigated on recrystallized and un-recrystallized Al–Cu–Li alloys by combining electron-backscatter-diffraction and micro-hardness mapping. The spatial heterogeneity of micro-hardness is found to be strongly dependent on the grain microstructure. Controlled experiments are carried out to change the pre-strain before artificial ageing. These experiments lead to an evaluation of the range of local strain induced by pre-stretching as a function of the grain microstructure and results in heterogeneous formation of the hardening T_1 precipitates.

1. Introduction

Recently developed Al–Li–Cu alloys, such as the AA2198 alloy, are well suited for high performance aerospace applications as they exhibit low weight, high strength and good thermal stability of their properties [1–5]. The thermo-mechanical process applied to these alloys consists of a series of hot processing stages (homogenization and hot rolling) followed by solution treatment, quench, pre-stretching and finally artificial ageing [6]. The grain microstructure and related crystallographic texture of the alloy depend on the details of the hot processing stages and are determined after the solution treatment. These process parameters affect the degree of recrystallization [7]. During artificial ageing, the AA2198 alloy strength increases dramatically through the precipitation of the T_1-Al_2LiCu phase. The T_1 precipitates form as high aspect ratio plates lying in the $\{111\}_{Al}$ planes and nucleate on dislocations [8,9]. Thus, pre-stretching the alloy is necessary to favor the formation of the T_1 phase [10] and the degree of pre-stretching has a strong influence on the kinetics of precipitation and related strengthening [11].

The crystallographic texture of these alloys, together with the anisotropic nature of the precipitates, is known to result in yield strength anisotropy [12–19]. However, the texture can also result in an inhomogeneous distribution of dislocations during the pre-stretching step thus creating an inhomogeneous hardening response during ageing treatment [14]. The aim of this paper is to identify quantitatively the origin of the inhomogeneity of the spatial distribution of strength by studying its magnitude in an Al–Li–Cu alloy with two different crystallographic textures.

Un-recrystallized rolled Al–Li–Cu alloys usually exhibit a strong brass texture $\langle 112 \rangle \{110\}$ [19,20]. Kim and Lee [14] pointed out that the uniaxial pre-stretching step resulted in a non-homogeneous distribution of dislocations depending on the activated slip planes. As T_1 nucleates on dislocations, it then resulted in an inhomogeneous distribution of precipitates thus contributing to yield strength heterogeneity. The link between crystal orientation and precipitation is clear as the nucleation and subsequent growth of T_1 strongly depends on the local dislocation density. However, to date, there is no quantitative study of the relationship between the range of precipitation inhomogeneity and the grain microstructure.

In the present work, the inhomogeneity of strengthening will be studied on two materials with significantly different crystallographic textures. The first specimen is unrecrystallized and thus has a pronounced rolling texture with long-elongated grains, while the second one is recrystallized and thus displays a weak texture with a distribution of equiaxed grains. We combine electron backscattered

* Corresponding author at: Institute for Frontier Materials, Deakin University, Geelong, Victoria 3217, Australia. Tel.: +61 3 52271481.
E-mail address: thomas.dorin@deakin.edu.au (T. Dorin).

diffraction (EBSD) with micro-hardness maps in order to investigate the local relationship between texture and strengthening. The results are then compared with experiments where the plastic strain during the pre-stretching operation is varied continuously in a controlled way. The obtained results are discussed in terms of inhomogeneity of pre-stretching throughout the grains, inhomogeneous precipitate kinetics and thus heterogeneous strengthening behavior.

2. Material and experimental procedure

Two sheets of AA2198 alloy were provided by Constellium Technology Center, Voreppe. The first sheet was 5 mm thick with a fully un-recrystallized grain structure and the second sheet was 1.4 mm thick with a fully recrystallized grain structure. The samples were first solution treated and water quenched. Right after quenching, the samples were pre-deformed, in the rolling direction, to a macroscopic tensile plastic strain of 2.5%. The samples were then naturally aged for seven days. The artificial ageing treatment was executed in an oil bath, starting with a heating ramp of 20 K h^{-1} to 155 °C, followed by an isothermal treatment at 155 °C. The samples were quenched into cold water at different times during the heat treatment and then analysed. The sample preparation for EBSD and micro-hardness consisted in a mirror polishing procedure that consisted in gradual grinding and diamond polishing steps down to colloidal silica ($\sim$0.01 μm).

The Vickers micro-hardness measurements were performed on a Wilson hardness Tukon 1102 fully automatic apparatus. A mass of 500 g was first used to measure the hardness evolution at 155 °C (indent diameter of 70–100 μm). A mass of 100 g was used for the hardness mapping (indent diameter of 30–40 μm). The electron back scattered diffraction (EBSD) measurements were conducted on a SEM-FEG ZEISS Ultra 55 apparatus. A scanning step of 1 μm was used for the EBSD acquisition.

Fig. 1a and b displays the inverse pole figure maps measured in EBSD on the two specimens. Note that these EBSD maps were acquired on a sample aged 7 h at 155 °C, however since the grain microstructure does not change during ageing at this temperature it is representative of the sample state during the pre-straining operation. The long elongated grains observed in the un-recrystallized state are typical of the rolling brass texture that prevails in this alloy. The ⟨110⟩ direction is observed to be dominant in the rolling plane. The recrystallized state shows an equiaxed distribution with grain sizes ranging from $\sim$20 μm to $\sim$500 μm and an average grain size of $\sim$150 μm.

From now on and for more clarity, recrystallized and un-recrystallized will respectively be denominated R and UR.

3. Evolution of micro-hardness during aging

The Vickers micro-hardness evolution was recorded during artificial ageing at 155 °C for both the R and UR materials. In order to get enough statistics, 20 indents were performed on each sample. Fig. 2a and b shows respectively the evolution of the average micro-hardness and its standard deviation for the two texture conditions. The micro-hardness first drops during the heating ramp. This phenomenon has previously been attributed to the dissolution of clusters [10]. The hardening kinetic is then similar in both cases with a slightly higher peak hardness for the R condition. The similarity in the hardness evolutions indicates that the grain morphology and texture has, on average, only a small effect on strengthening.

However, in contrast to the average hardness, the standard deviation of the hardness measurements shows a very different behavior in the UR and R conditions. For early ageing times, similar standard deviations are observed but the values rapidly differ after a few hours at 155 °C. For the case of the UR state, the standard deviation is relatively stable between 1 Hv and 3.5 Hv with no clear evolution throughout the heat treatment. In contrast, the R state displays a clear evolution throughout the heat treatment. The standard deviation first increases to a maximum of $\sim$12 Hv after 7 h at 155 °C and then decreases towards the end of the heat treatment. The standard deviation reached after 7 h at 155 °C for the R specimen is significant as it corresponds to approximately 10% of the average value. The evolution of the standard deviation shows a clear effect of grain microstructure on the hardness dispersion with a much more inhomogeneous distribution of hardness kinetics in the R sample as compared to the UR state. The extreme case of 7 h at 155 °C presents the strongest heterogeneity and was thus selected for further investigations.

4. EBSD and hardness mapping

EBSD and hardness mapping were conducted on the same areas on both the UR and R conditions after a heat treatment of 7 h at 155 °C (see Fig. 1a–d).

The micro-hardness map consists in 20 lines of 24 indents. The indents were regularly spaced every 100 μm and a load of 100 g was used, resulting in an indent diameter of about 35 μm, thus generally smaller than the grain size. The distance between indents was chosen to be large enough in order to avoid undesired interactions between the indents' strain fields. Fig. 1c and d displays the hardness maps, generated from the hardness measurements, in the form of iso-hardness regions. The average hardness is found to be 136 Hv and 129 Hv respectively for the UR and R state. These values differ slightly from one another but remain in good agreement with the average hardness of 130 Hv measured previously after 7 h at 155 °C (Fig. 2). As observed previously, the dispersion in the hardness measurements is significantly different in both conditions. The standard deviations are found to be 8.1 Hv and 3.5 Hv respectively for the R and UR conditions. We find the same trend as for the results of Fig. 2, even though the difference in dispersion is somewhat smaller in this second set of measurements. This small discrepancy can be explained by a larger measurement statistics in the second experimental dataset, or by the change in indenter load.

While the spatial distribution of hardness seems to follow the same morphological characteristic as the grain structure, it is not possible to directly correlate single grains with a corresponding hardness region. Indeed, the hardness measurement depends on many parameters such as the presence of grain boundaries buried below the apparent grain, and the level of plastic strain is not expected to be completely uniform in each grain. Therefore, to complete this qualitative comparison, it was chosen in the following to quantify the dispersion of plastic strain introduced in the material during the pre-stretch operation, by the evaluation of the strengthening kinetics during the precipitation heat treatment as a function of pre-strain.

5. Discussion

The precipitation of the T_1 phase strongly influences the yield strength of this type of Al–Li–Cu alloys. As the T_1 precipitates nucleate on dislocations, the pre-stretching step is important. We have shown in a previous study [11] that varying the amount of pre-strain had a strong influence on the precipitation kinetics, namely the evolution of precipitate volume fraction and of the related strengthening was faster, the higher the pre-strain. The

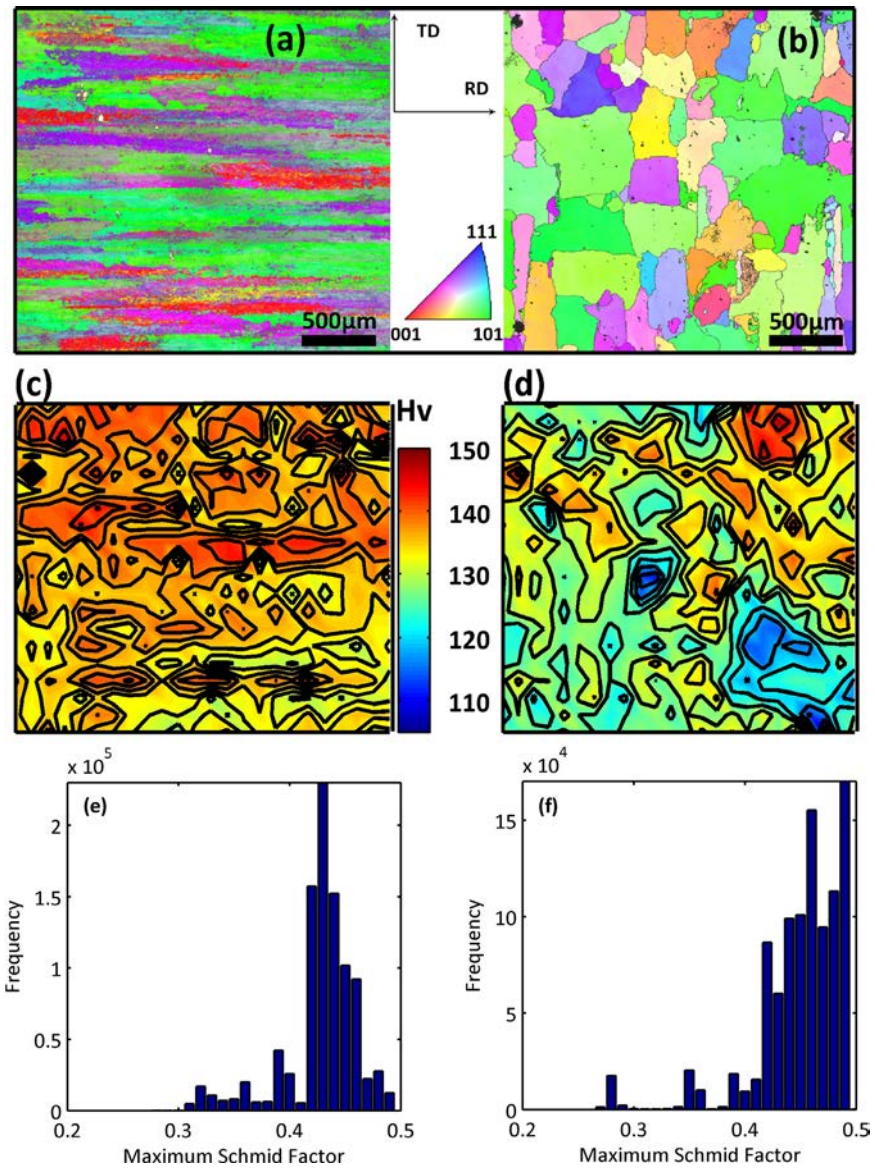

Fig. 1. EBSD images of an AA2198 alloy with (a) an UR texture and (b) with an R texture and corresponding micro-hardness mapping of the same areas (c) and (d). (e) and (f) The maximum Schmid factor distributions for respectively the UR and R states extracted from the EBSD maps.

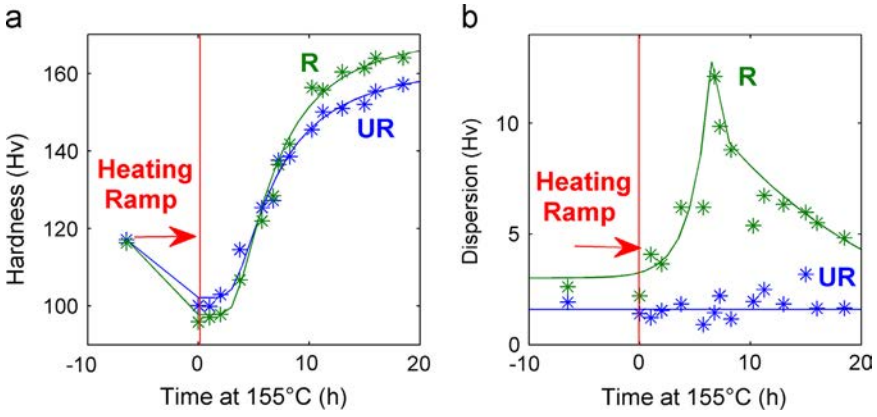

Fig. 2. (a) Vickers micro-hardness evolution as a function of ageing time at 155 °C for both the UR and R AA2198 and (b) evolution of the standard deviation for both conditions.

distribution of dislocations in a polycrystal subjected to relatively modest levels of plastic strain (2.5% on average) can be highly heterogeneous depending on the distribution of the maximum Schmid factors through the microstructure, which is indicative of the local applied stress necessary for activating plasticity. It is expected that the UR microstructure presents a relatively uniform

distribution of Schmid factors regarding a tensile test performed in the rolling direction (such as done here during the stretching step), thus favouring a relatively homogeneous distribution of dislocation density in the material during stretching. The recrystallized material, however, can be expected to have a distribution of Schmid factors closer to a random texture, thereby favouring a more heterogeneous distribution of plastic strain during the stretching step. For each data point of the EBSD maps, we determined the maximum Schmid factor with respect to stretching in the rolling direction. The distribution of these maximum Schmid factors is shown in Fig. 1e and f. In the UR material the distribution is relatively narrow around 0.43 (average value) whereas in the R material the distribution is more flat: a large number of points have a Schmid factor around 0.5, and some have a very low factor smaller than 0.4. Although the distribution of Schmid factors is not self-sufficient to predict the distribution of plastic strain through the polycrystal, these distributions must result in a more homogeneously distributed plastic strain in the UR microstructure as compared to the R microstructure. In a further step, we will now estimate from the extent of the hardness dispersion, the distribution of plastic strain experienced throughout the two materials under study.

In a recent study on the AA2198 alloy [11], the kinetics of T_1 precipitation was quantitatively measured for samples having experienced several levels of pre-strain. The kinetics was revealed to be significantly different depending on the initial pre-stretch thus resulting in different strengthening kinetics. The yield strength evolutions for three pre-deformation 0.5%, 2.5% and 12% is reported in Fig. 3a (re-plotted from [11]). It can be noticed that despite significantly different kinetics, the peak yield strength is similar for all three pre-deformations. To estimate the dispersion in the strengthening kinetics between these three levels of pre-stretch, we calculated a dispersion between the 3 conditions from the 3 JMAK-type fits as follows:

$$\text{Dispersion} = \sqrt{\frac{(\text{fit}_1 - \text{Avg})^2 + (\text{fit}_2 - \text{Avg})^2 + (\text{fit}_2 - \text{Avg})^2}{3}} \quad (1)$$

where fit_1 fit_2 and fit_3 are the fits for the three pre-deformation 0.5%, 2.5% and 12%, respectively. Avg is the average from the three previous fits. The evolution of this dispersion is displayed in Fig. 3b and evolves in fair agreement with the standard deviation for the R state (Fig. 2b). The standard deviation evolves to a maximum of 85.3 MPa after 8 h at 155 °C and then decreases. This translates to a maximum of approximately 26 Hv if a rough conversion, with the formula $\text{Hv} = 0.3 \times \text{YS}$ (where Hv is the hardness and YS is the yield stress), is applied. This maximum value is much higher than the standard deviations of 8.1 Hv and 3.5 Hv, found in the previous part for the R and UR samples, revealing that the range of pre-stretching through the grains is smaller than [0.5%,12%]. It is interesting to notice that the maximum of standard deviation reported in Fig. 2b occurs after approximately the same duration of ageing as reported in Fig. 1. This maximum in the transient reveals that the peak in heterogeneous strengthening induced by precipitation occurs after approximately 8 h at 155 °C for the A2198 alloy. This time corresponds to the time where the material with the largest amount of pre-stretch has almost completed its maximum strengthening increment, while the material with the lowest amount of pre-stretch as merely started to strengthen. For shorter ageing times precipitation is not yet significant in any materials and therefore the dispersion of hardness is small, and for longer ageing times precipitation becomes completed for all materials and the dispersion of hardness is again small.

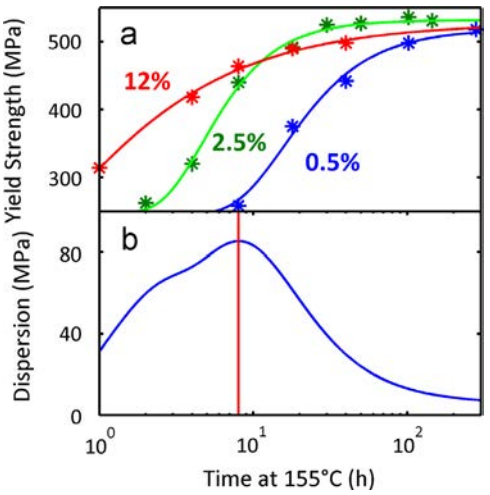

Fig. 3. (a) Yield strength evolution at 155 °C for the AA2198 alloy for three pre-deformations 0.5%, 2.5% and 12% (taken from [11]) and (b) standard deviation of yield strength as a function of time at 155 °C calculated from the JMAK fits from (a).

Vasudevan and co-workers [13] emphasized a similar phenomenon, although less straightforward to interpret, in the strengthening kinetics of the AA2090 alloy by comparing the evolution of the following yield strength ratios $\sigma(45°)/\sigma(0°)$ and $\sigma(45°)/\sigma(90°)$, where the angles are in reference to the rolling direction. These ratios would be expected to evolve monotonically in isotropic alloys during ageing. Instead, they observed a non-monotonical evolution with a maximum in the transient after 2 h at 163 °C before the evolution became monotonic again.

On the other hand, Crooks et al. [17] only compared the yield strength in As-cast and in T8 states for different pre-stretch conditions and then concluded that T_1 had only a weak effect on strengthening heterogeneity. Our current findings shed some more light on these results, where the authors have drawn that

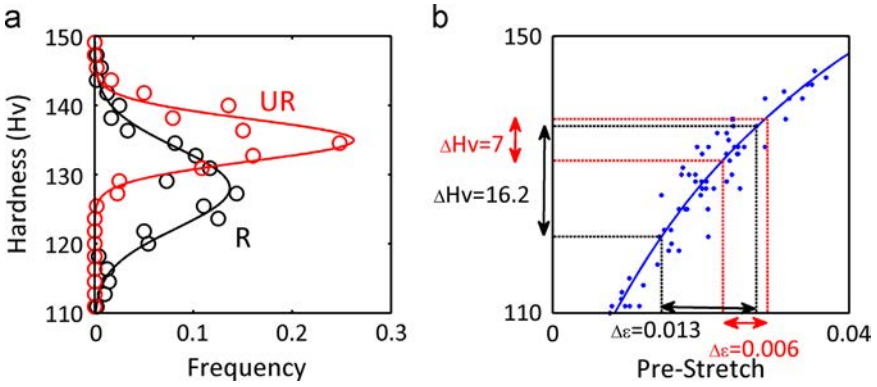

Fig. 4. (a) Hardness distributions measured on an UR and a R AA2198 specimens and (b) hardness as a function of pre-stretch after 7 h of heat treatment at 155 °C.

conclusions on the basis of the final yield strength while we have shown that it is during the formation of precipitates, and not on the finale state T8, that the effect was greatest.

The hardness measurements from Fig. 2c and d were arranged into classes and the distributions were fitted with a normal distribution function (see Fig. 4a). This representation highlights the higher dispersion in the case of the R condition. In order to quantify the pre-stretch variations from one grain to another, we used a tensile sample of varying cross-section (as-described in [11]) to create a pre-stretch gradient. The sample was pre-stretched so that to obtain a deformation gradient from 0% to 4% (as measured by digital image correlation). The sample was then heat treated 7 h at 155 °C and the hardness measured along the sample. The hardness evolution as a function of the applied pre-stretch is displayed in Fig. 4b. The spread in hardness of respectively 7 Hv and 16.2 Hv for the UR and R states can then be translated into pre-stretching ranges of 0.6% and 1.3%.

6. Conclusion

In this study we have quantified the heterogeneity of precipitation strengthening in the AA2198 alloy as a function of the grain microstructure and related it to the heterogeneity of the distribution of plastic strain during the stretching step that follows the quench from the solution heat treatment. It was demonstrated that pre-stretching results in a significant heterogeneity of hardening in between the grains, which is more pronounced in a recrystallized microstructure as compared to an un-recrystallized microstructure. The pre-stretching spread was quantified on the AA2198 alloy for two specific texture conditions.

References

[1] J. Williams, E. Starke Jr., Acta Mater. 51 (2003) 5775–5799.
[2] T. Warner, Mater. Sci. Forum 519–521 (2006) 1271–1278.
[3] R. Rioja, J. Liu, Metall. Mater. Trans. A 43A (2012) 3325–3337.
[4] F. Tchitembo Goma, A. Bois-Brochu, C. Blais, J. Boseli, M. Brochu, Proceedings of the ICAA13: 13th International Conference on Aluminum Alloys, Pittsburgh, 2012.
[5] A. Daniélou, J. Ronxin, C. Nardin, J. Ehstrom, Proceedings of the 13th International Conference on Aluminium Alloys, Pittsburgh, PA, TMS, Warrendale, PA, 2012, pp. 511–516.
[6] A. Heinz, A. Haszler, C. Keidel, S. Moldenhauer, R. Benedictus, W. Miller, Mater. Sci. Eng. A 280 (2000) 102–107.
[7] D. Tsivoulas, J. Robson, C. Sigli, P. Prangnell, Acta Mater. 60 (13–14) (2012) 5245–5259.
[8] B. Gable, A. Zhu, A. Csontos, E. Starke Jr., J. Light Met. 1 (2001) 1–14.
[9] T. Dorin, A. Deschamps, F. De Geuser, W. Lefebvre, C. Sigli, Philos. Mag. 94 (10) (2014) 1012–1030.
[10] B. Decreus, A. Deschamps, F. De Geuser, P. Donnadieu, C. Sigli, M. Weyland, Acta Mater. 61 (2013) 2207–2218.
[11] T. Dorin, A. Deschamps, F. De Geuser, C. Sigli, Acta Mater. 75 (2014) 134–146.
[12] A. Vasudevan, W. Fricke Jr., R. Malcolm, R. Bucci, M. Przystupa, F. Barlat, Metall. Trans. A 19A (1988) 731–732.
[13] A. Vasudevan, M. Przystupa, W. Fricke Jr., Scr. Metall. Mater. 24 (1990) 1429–1434.
[14] N. Kim, E. Lee, Acta Metall. Mater. 41 (3) (1993) 941–948.
[15] K. Jata, A. Hopkins, R. Rioja, Mater. Sci. Forum 217–222 (1996) 647–652.
[16] K. Jata, S. Panchanadeeswaran, A. Vasudevan, Mater. Sci. Eng. A 257 (1998) 37–46.
[17] R. Crooks, Z. Wang, V. Levit, R. Shenoy, Mater. Sci. Eng. A 257 (1998) 145–152.
[18] S. Hales, R. Hafley, Mater. Sci. Eng. A 257 (1998) 153–164.
[19] Q. Contrepois, C. Maurice, J. Driver, Mater. Sci. Eng. A 527 (2010) 7305–7312.
[20] C. Maurice, J. Driver, Acta Mater. 45 (11) (1997) 4627–4638.